The effect of phase angle on crack growth mechanisms under thermo-mechanical fatigue loading

J. Jones[*], M. Whittaker[*], R. Lancaster[*], C. Hyde[+], J. Rouse[+], B. Engel[+], S. Pattison[**], S. Stekovic[++], C. Jackson[“], H.Y. Li[“]

[*] Institute of Structural Materials, Bay Campus, Swansea University, SA1 8EN. (UK)
[+] Department of Mechanical, Materials and Manufacturing Engineering Faculty, Nottingham University, NG7 2RD. (UK)
[**] Rolls-Royce plc, Elton Road, Derby, DE24 8BJ. (UK)
[++] Department of Management and Engineering, Linköping University. (Sweden)
[“] School of Metallurgy and Materials, University of Birmingham, Edgbaston, Birmingham B15 2TT, UK

Abstract

The current paper describes TMF crack growth behaviour in an advanced nickel-based superalloy. Changes in behaviour are examined which occur as a function of the phase angle between applied stress and temperature. The fractography of the failed specimens reveals changes from transgranular to intergranular growth between high and low phase angle tests as a result of the onset of high temperature damage mechanisms. More targeted testing has also been undertaken to isolate the contributions of these mechanisms, with specific transitions in behaviour becoming clear in 90° diamond cycles, where dynamic crack growth and oxidation strongly interact.

Keywords: Thermo-mechanical fatigue; phase angle; creep; oxidation

Introduction

In situations where non-isothermal service environments occur, thermo-mechanical fatigue (TMF) has been widely recognised as a significant damage mechanism at elevated temperatures in a number of alloy systems. Examples of components where TMF is prevalent include pressure vessels and pipes in the power generation sector, engine components in the automotive industry and turbine discs and blades in the modern jet engine. For over 40 years work has continued towards developing modelling approaches to replicate these service environments, often with only limited success. The complex nature of interplay between fatigue, creep and environmental damage mechanisms means that it is often difficult to extrapolate TMF lives from isothermal data. In addition to traditional parameters such as strain range, loading ratio and applied temperature, further parameters are introduced when TMF is present such as peak and range of the temperature cycle and phase angle, which complicate constitutive relationships and only partial solutions are derived, limiting the breadth of the relationship.

Due to the nature of the thermal cycle, and the restrictions on heating and cooling rates, cycle times in all of these tests far exceed those of traditional isothermal tests where stress or strain can be varied rapidly. Out of practicality much of the TMF data in the open literature therefore has fatigue lives within the short life regime of the S-N curve, and often towards the shorter life end.

As such, when attempting to predictively model TMF data with shorter lives, it is often further complicated by the fact that fatigue crack propagation can no longer be considered to be an insignificant portion of the total fatigue life. Therefore, attempts to rationalise this short life data often does not fit into broader assumptions about TMF behaviour [1], meaning that there is a critical requirement to generate crack propagation data under representative non-isothermal

environments. For instance, the work by Marchionni et al [2], reproduced here in **Figure 1**, was conducted as part of the Code of Practice development, [3] investigating TMF effects in Nimonic 90. The generated results were counterintuitive to the model proposed by Lancaster et al [1] where mean stress evolution was shown to play a significant role in TMF life, and in this case showed that increased mean stresses did not produce a reduction in fatigue life. Instead, In-Phase (IP) tests were shown to have consistently shorter TMF lives than Out of Phase (OP) experiments. In the review by Lancaster et al [1] it was suggested that the short TMF lives, ranging from only 80-2000 cycles, were dominated by fatigue crack propagation rather than crack initiation behaviour.

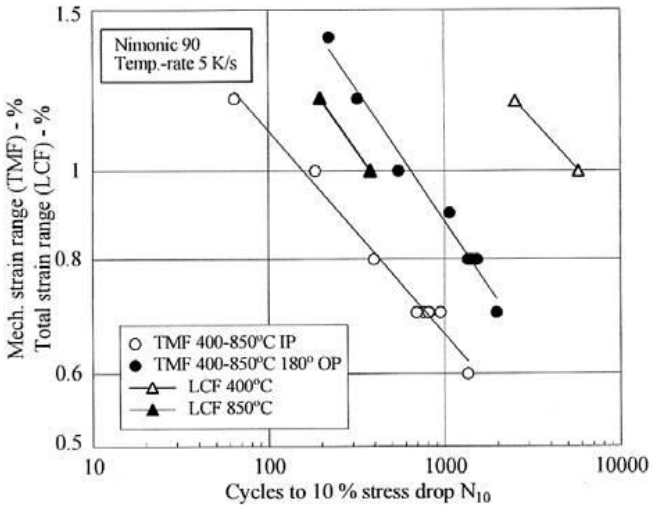

Figure 1. *Comparison of TMF and isothermal fatigue (IF) lives in Nimonic 90 with a peak cycle temperature of 850°C. [2]*

It is clear then that for short fatigue lives, under TMF loading, as in isothermal fatigue, the contribution of crack propagation must be considered as part of a modelling approach. Therefore, appropriate test methodologies require development in order to generate consistent TMF crack propagation data. In what is clearly an emerging field, only a limited amount of work has been undertaken, yet this has proven to be useful in providing a background for the current work. Early work utilised similar setups but focussed on steels with a peak temperature of 600°C [4], whereas the detailed work by Marchand [5] and Gemma [6] provided more extensive studies of TMF crack growth in nickel based alloys mainly employing strain control conditions. Following this only sporadic pieces of work are found in the literature.

More recently focus has returned to the area of TMF crack propagation, presumably following on from the improved testing procedures and understanding gathered by the TMF strain controlled code of practice [3, 7], which helps to develop a pathway for this type of testing through its detailed evaluation of non-isothermal testing. Moverare and Gustafsson [8] investigated TMF crack growth effects in IN718 using a single edge notch specimen placed in an induction coil, with crack growth monitored by a compliance based method. The authors commented that an appropriate temperature distribution was achieved in the work provided heating and cooling rates were kept relatively low (1°C/sec in this case) and that an output of the work was the ability to correlate isothermal and TMF crack growth rates in the material. Further work by Moverare [9] using similar methodologies on the cast nickel blade alloy IN792 also investigated the effect of dwell periods under TMF loading, and showed interesting parity between IP and OP tests with a 5 minute dwell period.

The issue of crack growth experimentation under induction heating has long been questioned, due to the risk of preferential crack tip heating. However, more recently the work by Palmer et al [10] has shown no significant effect of this in the nickel superalloy RR1000, and also in the titanium alloy Ti6246. Whilst alternative approaches such as lamp furnaces offer an alternative heating source, induction coils require less capital expenditure and provide the opportunity for easier access to the test specimen, allowing for additional investigation through extensometry, thermography and digital image correlation. Crack measurement techniques are also made easier by the use of induction heating with optical measurements possible. However, compliance based methods such as those used by Moverare [11] can be used in either setup, as can direct current potential drop (DCPD) techniques. In the case of DCPD however, care should be taken to avoid interference with the induction field if testing is conducted in a coil setup.

Perhaps the first systematic study of the effects of phase angle on fatigue crack growth rates was performed by Pretty et al [12] in which fine grained (FG) RR1000 growth rates were recorded in an induction coil system. The main conclusions of this work were that broadly speaking, TMF crack growth rates could be inferred from, and rationalised by, isothermal crack growth data produced at the temperature at which peak stress occurred in the test (i.e. 300°C for OP, 700°C for IP). Cycle times however proved important, particularly in IP crack growth where additional time dependent failure mechanisms (creep and oxidation) influenced crack growth rate. Furthermore, the influence of these mechanisms was shown to be important in clockwise and anticlockwise diamond tests (+90°CW and -90° ACW tests) where cycle direction led to changes in crack growth behaviour as time dependent oxidation at the crack tip interacted with the fatigue damage mechanism.

The current work seeks to further develop the concepts explored by Pretty [12] in the same alloy, albeit in a coarser microstructure, which is often generated in order to provide greater resistance to creep and oxidation at high temperatures. Higher peak cycle temperatures have also been employed to provide a more aggressive TMF cycle where the interactions of fatigue, creep and environment can be evaluated in more detail, with the first stages of a modelling approach also considered based on these results.

Material

The material utilised for this experimental research was predominantly the polycrystalline coarse-grained (CG) variant of the γ/γ' strengthened Ni-base superalloy, RR1000, developed and supplied by Rolls-Royce plc. The fine grained (FG) variant will also been investigated and compared. The mechanical properties of the alloy are principally governed by the volume fraction and size of the γ' precipitates, the main strengthening mechanism of the alloy, as well as the energy associated with the anti-phase boundary (APB) created in the γ' phase when plastically deformed [13]. Typically, the superalloy has a coarse grain size of 30-50μm and a fine grain size of approximately 10 μm. The nominal compositions are provided in **Table 1**.

Table 1. *Nominal Compositions of RR1000 in Weight %. [14]*

	Ni	Co	Cr	Mo	Ti	Al	Ta	Hf	Zr	C	B
RR1000	Bal	18.5	15.0	5.0	3.6	3.0	2.0	0.5	0.06	0.03	0.02

Experimental procedure

A rectangular section, corner cracked specimen design has been employed throughout the entirety of this research, inclusive of prior thermal profiling procedures. The test piece has a 0.35mm ±0.01mm single edge, corner starter notch machined in using a diamond edge sawblade.

Thermo-mechanical fatigue crack growth (TMFCG) testing was undertaken on two bespoke test setups. The first setup comprises of a 100kN servo-hydraulic test frame, utilising a Zwick CUBAS control system. A Trueheat 10-kW induction heating system is utilised to deliver rapid heating rates through a 4mm diameter copper tube, shaped into a non-uniform multi-turn longitudinal field helical coil with an approximate external diameter of 60mm. Rapid cooling rates were enabled through forced air cooling using four Meech pneumatic air amplifiers with their output controlled through proportional solenoid valves. Temperature feedback is provided through a 0.2mm diameter N-type thermocouple, spot welded at the centre of the 20mm gauge length on an opposing face to the starter notch. The setup is displayed in **Figure 2a**.

The second experimental system comprises of a 100kN servo-electric test frame, utilising a DARTEC control system. A 2nd generation radiant lamp furnace (RLF) was designed in collaboration with Severn Thermal Solutions Ltd to generate rapid heating rates similar to that of an induction coil. The 12kW RLF is a standard split body design with each half containing three horizontally mounted lamps. Three independently controllable heating zones allow for accurate temperature control and profiling, whist built-in internal compressed air cooling delivers the rapid cooling rates required by the complex TMF waveforms. Again, temperature feedback is provided through a 0.2mm diameter N-type thermocouple, spot welded at the centre of the 20mm gauge length on an opposing face to the starter notch. This setup is presented in **Figure 2b**. This TMF system has been designed with thermography temperature control at the forefront of the design specification. More information on this is design is given by Jones [15].

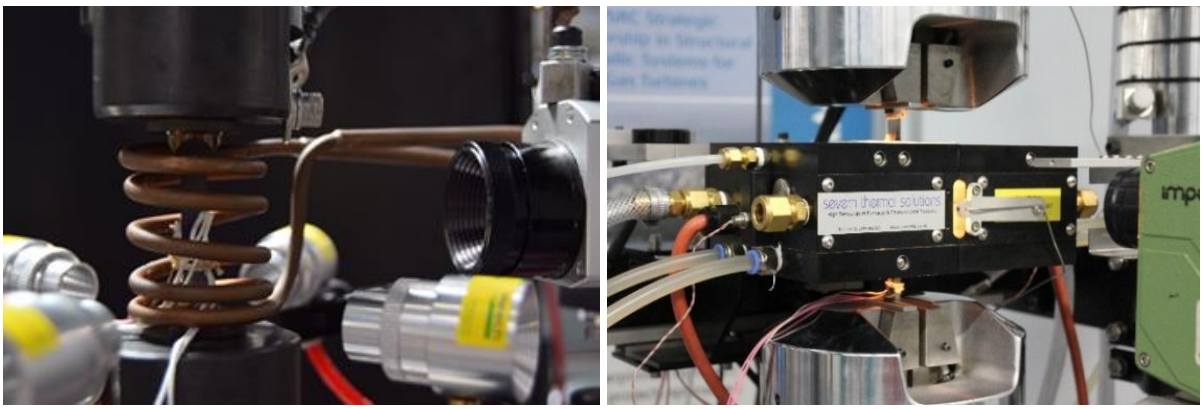

Figure 2: *Thermo-mechanical fatigue crack growth test setups utilised during this research. Non-uniform multi-turn longitudinal field helical induction coil and air amplifier combination (left). 2nd generation radiant lamp furnace (RLF) and internal forced air-cooling combination (right).*

A Dirlik control system interfaces together with the setups described above to record crack length against number of cycles (*a* vs *N*) readings through pulsing a 10 A signal and utilising the direct current potential drop technique (DCPD). This is then converted into *da*/*dN* data by using the incremental polynomial method, as described in the ASTM 647 appendixes, standard test method for measurement of fatigue crack growth rates [16].

Prior to any testing, rigorous thermal profiling was undertaken using six 0.2mm diameter type-N thermocouples. The thermocouples were spot welded at the centre gauge location on each of the

four rectangular specimen faces to realise the radial heating gradient. A further two thermocouples were spot welded 5mm above and below a centre thermocouple to generate axial temperature distributions. As no TMFCG standard currently exists, the authors employed the stringent temperature limits imposed by the governing TMF strain and stress control standards [17-19]. A typical temperature distribution of ±3°C was achieved, as given in **Figure 3**.

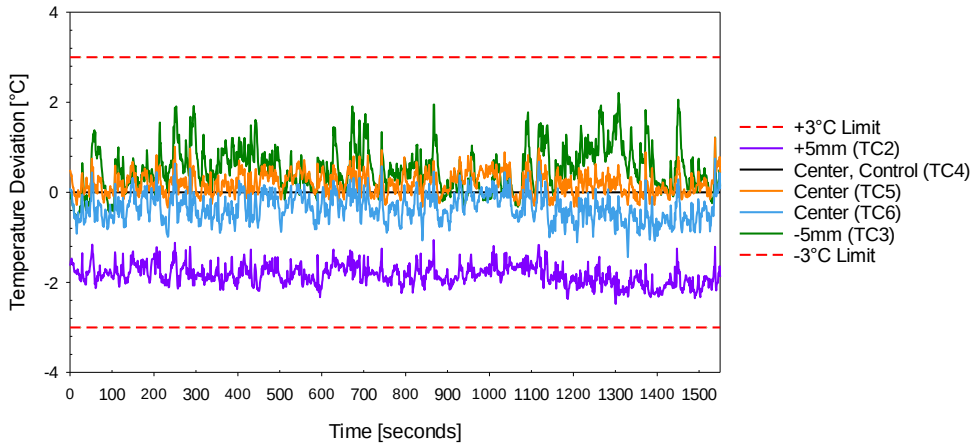

Figure 3: *Temperature distribution associated with non-uniform multi-turn longitudinal field helical coil, showing a spread of +/-3°C in temperature across the critical volume of material around the crack.*

All testing employed a triangular R=0 waveform, with a peak stress of 500MPa and a temperature range of 400-750°C, with heating and cooling rates at 10°C/s. However, the effect of increasing the peak temperature and decreasing the minimum temperature has also been explored from 775°C (peak) to 300°C (minimum) respectively. Testing has explored a range of phase angles between temperature and mechanical load, including in-phase (IP), out of phase (OP), as well as clockwise (90) and anti-clockwise (-90) diamond cycles. Further information regarding phase angles utilised in TMF crack testing is available in previous work [12, 20].

Results

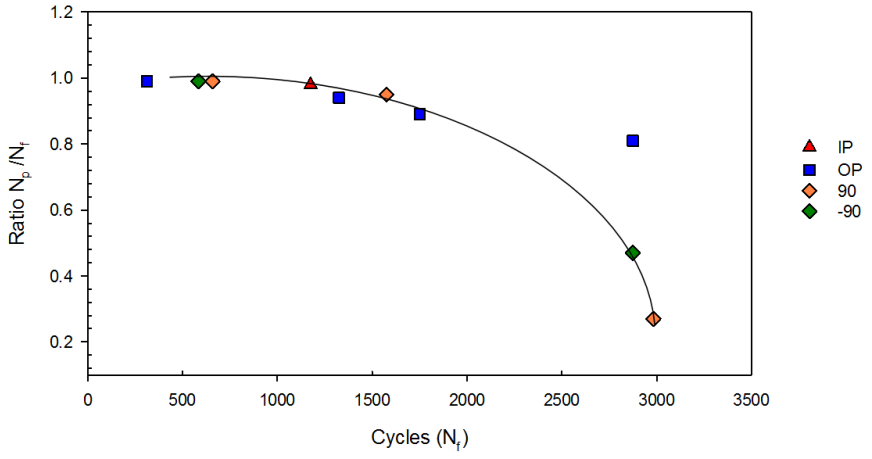

Figure 4. *Ratio of number of cycles in propagation/total life against total cycles to failure under TMF loading at 300-700°C in fine grained RR1000.*

Figure 4 presents the results from the strain control TMF tests on FG RR1000. The graph illustrates the ratio of the number of cycles in propagation over total life (N_p/N_f) as calculated using striation counts from the respective fracture surfaces under electron microscopy. The results encompass diverse phase angles and strain range test combinations. The clear decreasing parabolic trend of the results suggests that the majority of test life is spent in propagation, with total lives less than approximately 2500 cycles. The N_p/N_f ratio can be argued to closely correlate with strain range baring a few exceptions particularly in high strain range tests where cracks may have initiated during the very first few cycles. In general, the initiation period of total test life becomes more dominant as strain ranges decrease below 1.2% and total cycle lifetimes are greater than 2500.

A clear effect of grain size on the isothermal and TMF performance of RR1000 has been identified and is given in **Figure 5a**. In order to provide a more representative comparison, isothermal tests were undertaken at the peak TMF cycle temperature, 750°C. Beginning with the isothermal results, the larger "coarse" grained variant visibly displays a significantly improved crack propagation performance over the smaller "fine" grained variant. Comparing the isothermal performance of both variants against their similarly grain sized counterparts, the IP TMF growth rate shows a similar trend. Although in both instances the IP TMF growth rate is higher than the isothermal, the growth rate is not significantly enhanced by the dynamic thermal environment and is indeed a result of the extended cycle time in the TMF test as shown by Pretty [12], with the TMF cycle being 80s as opposed to the 4 second isothermal cycle. An extended period at "high" temperatures in the TMF test leads to a stronger influence of time dependent mechanisms such as creep and environmental damage and this increases the growth rate.

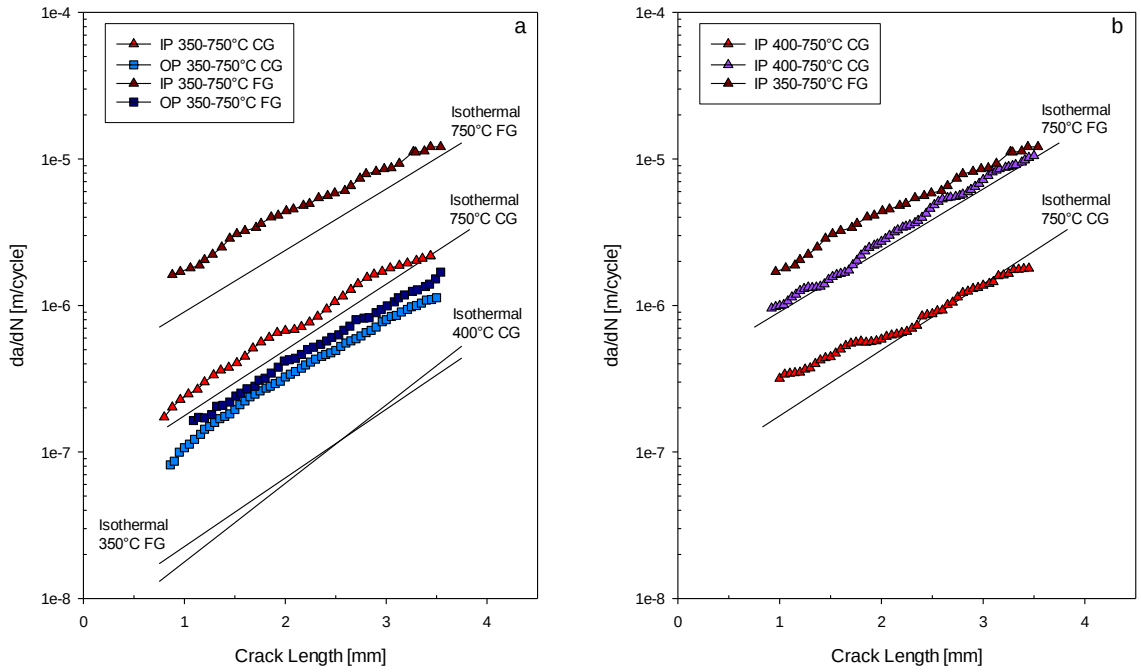

Figure 5: *Effect of grain size on FG and CG RR1000 crack growth rates vs. stress intensity range under TMF loading. a) IP and OP crack growth rates for FG and CG RR1000 variants under 350-750°C thermo-mechanical loading. b) IP crack growth rates for FG and CG RR1000 variants under 350-750°C and 400-750°C thermo-mechanical loading respectively.*

When comparing the growth rates of the two variants under TMF conditions, there is a similar trend to that observed in the isothermal comparison. The larger CG variant displays a superior crack growth resistance to that of the FG material, however the spread of the results under the diverse phasing is interesting. It is clearly noticeable that significant differences have occurred between two

tests performed under the same IP conditions in CG RR1000, **Figure 5b**. This level of variation was not seen in any experiments performed in FG RR1000, nor in OP tests in CG RR1000, indicating that the large grain size variant shows sensitivity to microstructure under the IP cycle at these temperatures.

In order to understand this effect, further microstructural characterisation has been conducted on four tests after testing. These four tests have shown varied crack growth resistance under identical IP conditions (400-750°C), the results of which are presented in **Figure 6a**. The size and distribution of γ' for the four tests are compared in **Figure 6b**. It can be clearly seen TC026 and TC004 had the finer and narrow distribution of secondary γ', which corresponds to poor crack growth resistance (faster crack growth rates under any given ΔK values); whereas coarser and wider distribution of secondary γ' give rise to better crack growth resistance. The sensitivity of crack growth resistance to microstructure observed here is consistent to that reported by Li et al [21]. For the temperature range tested, both environmentally assisted crack growth and creep damage can accelerate crack growth (compared to isothermal fatigue crack growth data at peak temperature). However, it is confirmed by fractographic observation that the acceleration of crack growth rates observed here result from a brittle environmental intergranular crack growth. Other microstructural parameters such as grain size have also been analysed but show little variation.

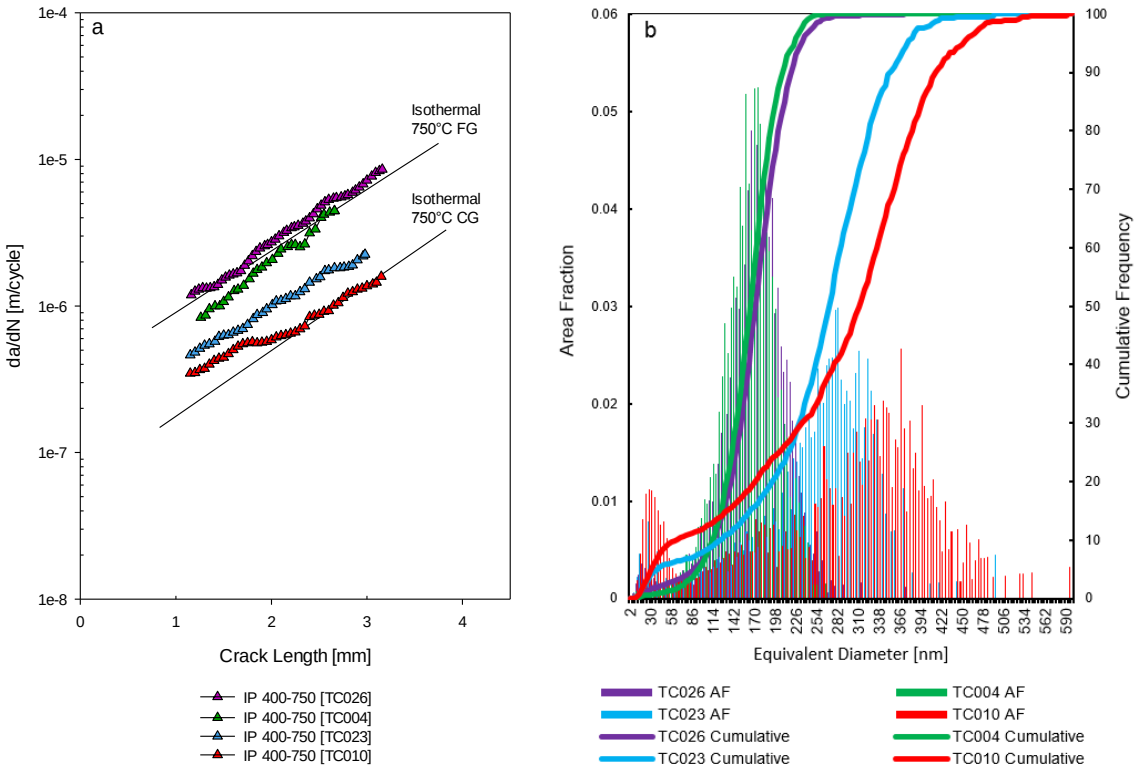

Figure 6. *Microstructural effects on CG RR1000 TMFCG rates. a) Four IP 400-750°C TMFCG Paris curves. b) Corresponding secondary γ'distributions of results displayed in a).*

A distinct difference is evident in the appearance of the fracture surfaces of the FG and CG variants of RR1000 due to grain size, as depicted in **Figure 7**. The two variants display a similar relationship between the phasing employed and the fracture mechanics of the crack growth. Under IP loading it is clear that intergranular crack growth dominates with characteristic triple points and a faceted appearance. The grain structure is clearly defined as the crack has progressed along the grain boundaries. In contrast, OP TMF loading induces dynamic transgranular crack growth across the

polycrystalline grain structure. Clear evidence of this is displayed on the smooth fracture surfaces with clear cleavage steps, river patterns and feather markings typical of transgranular growth.

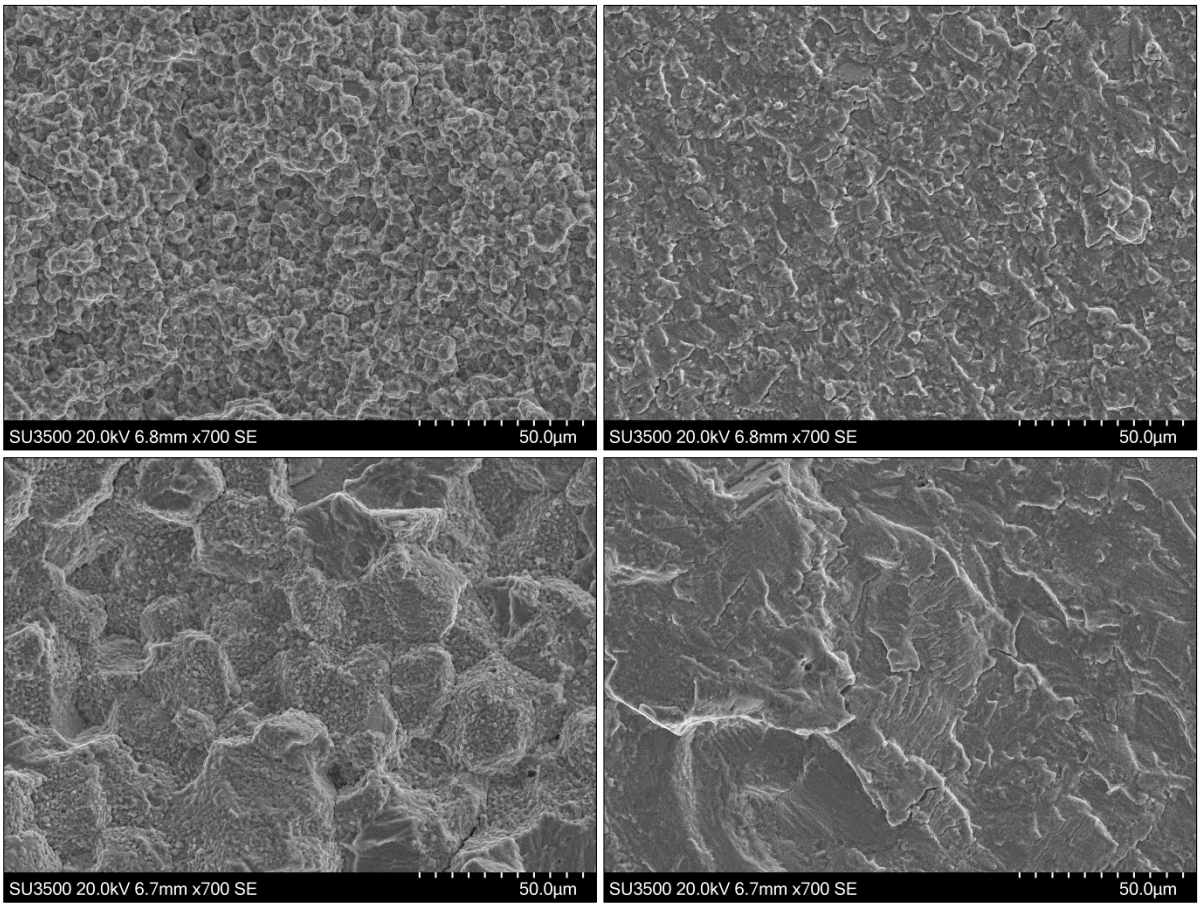

Figure 7: *Fracture surfaces of IP and OP, TMF experiments displayed in **Figure 5a** at 350-750°C on FG and CG variants of RR1000 at x700 magnification. IP FG (top left), OP FG (top right), IP CG (bottom left) and OP CG (bottom right).*

The effect of cycle temperature on the TMFCG rate of both the FG and CG variants was also investigated. In the CG variant this was accomplished by increasing and decreasing T_{Max} (by 25°C) and T_{Min} (by 50°C) of the baseline 400-750°C triangular TMF cycle accordingly. The result of increasing the peak cycle temperature by 50°C to 750°C on FG RR1000 under IP and OP loading is given in **Figure 8a**. Under OP TMF loading conditions the increase in temperature appears have minimal effect on the crack growth rate. A minor increase in growth rate is evident under IP loading. **Figure 8b** shows a similar comparison for the CG variant where the T_{Max} of the cycle is increased, in this case by 25°C to 775°C. A similar approach where the T_{Min} of the cycle was reduced by 50°C to 350°C showed no significant variation in growth rates and so has not been included here.

Interestingly, in CG RR1000, when the peak cycle temperature increases, an increase in crack growth rate in OP tests is also seen. Whilst this increase in growth rate is small, it has been shown consistently in a number of repeat tests. Furthermore, similar increases in growth rate were observed when a dwell period was added at peak stress in OP tests (400-750°C). Dwell periods of 5, 60 and 120 seconds have also been investigated and were shown to increase the growth rate in a linear manner with dwell time. The most significant increase, from the 120s dwell test, is included in **Figure 8b**.

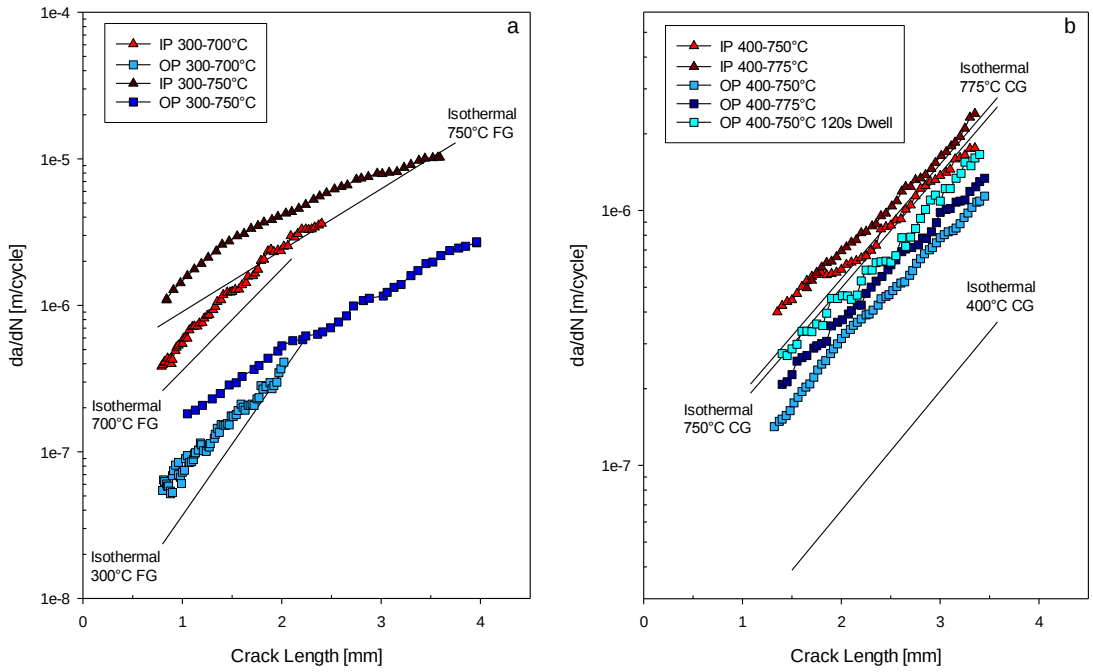

Figure 8: *Effect of Peak Cycle Temperature on FG and CG RR1000 TMFCG rates. a) FG RR1000 IP and OP crack growth rates under 300-700°C and 300-750°C thermo-mechanical loading. b) CG RR1000 IP and OP crack growth rates under 400-750°C and 400-775°C thermo-mechanical loading.*

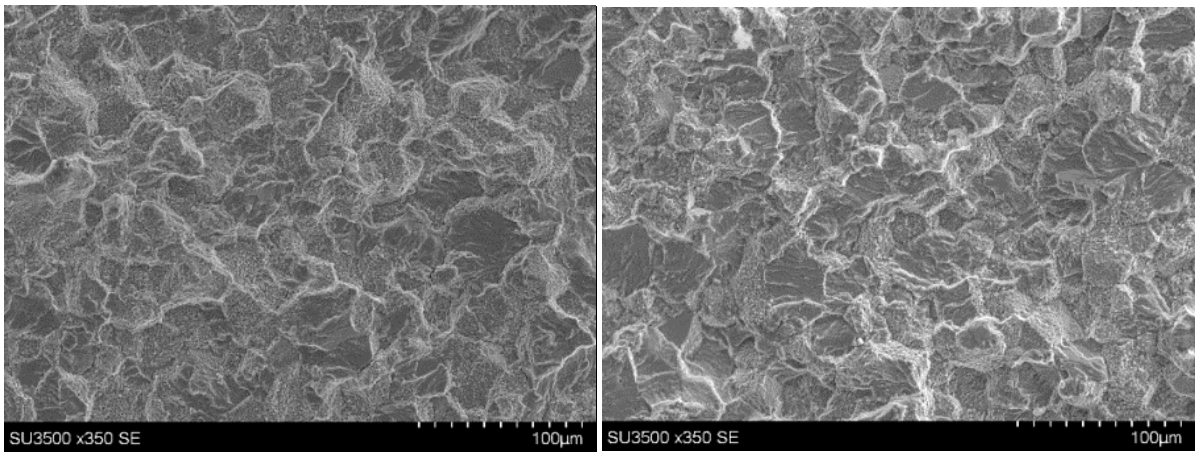

Figure 9: *IP TMF coarse grained RR1000 fracture surfaces at 350x magnification under ΔT=400-750°C (left) and ΔT=400-775°C (Right).*

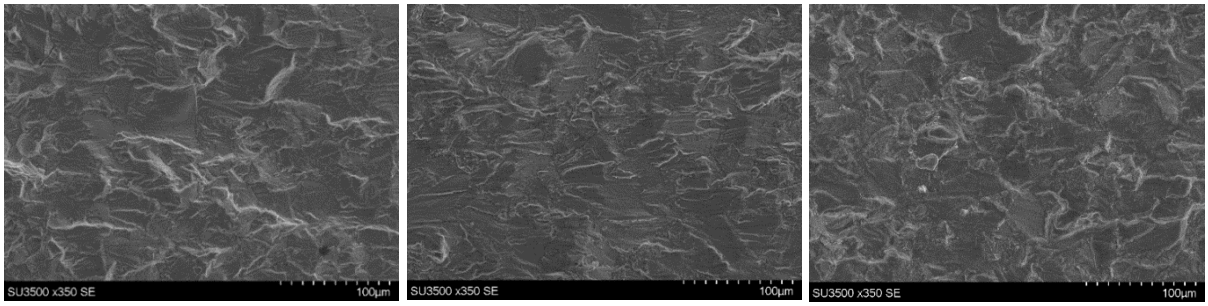

Figure 10: *OP TMF CG RR1000 fracture surfaces at 350x magnification under ΔT= 400-750°C no dwell (left), ΔT= 400-775°C no dwell (centre) and ΔT= 350-750°C 120s dwell at peak temperature (right).*

As expected, IP tests continue to be dominated by intergranular crack growth, **Figure 9**. **Figure 10** shows the fracture surface of the CG RR1000 specimens for both 400-750°C and 400-775°C cycles, and it is evident that crack growth occurs in a transgranular manner, indicating in particular that oxidation has not played a significant role in this increased crack growth rate. In the previous work by Pretty et al [12] oxidation was shown to significantly influence crack growth rates and was easily identified from a transition from transgranular to intergranular cracking. In the current work however, it appears that significant levels of oxygen, capable of influencing fracture behaviour through environmental effects are unable to penetrate to the crack tip when the minimum load is applied at the peak cycle temperature in the OP test.

It is therefore hypothesised that the increase in crack growth rate is due to the influence of creep at high temperature. In particular the unloading of the specimen induces significant compressive stresses at the crack tip, which relax at the peak temperature in the OP cycle. In both the cases of the higher cycle temperature (400-775°C) and the dwell tests (400-750°C) more significant relaxation of these compressive stresses occurs. Therefore, as loading occurs and the crack opens, greater increments of strain occur at the crack tip, and the crack growth rate increases. The effect is not seen in FG RR1000 because of the lower rate of strain hardening and the material is less sensitive to reduction in compressive strain prior to loading.

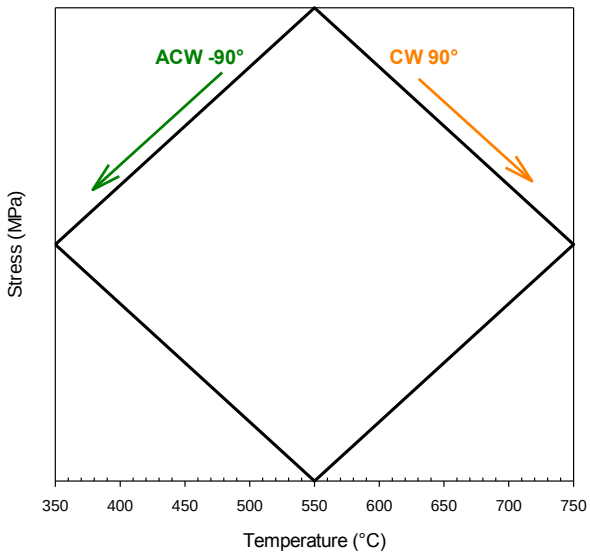

Figure 11: *Direction of diamond cycles applied in FG RR1000.*

Through this increased crack growth rate in OP tests, the interaction between fatigue and creep at high temperatures has been clearly demonstrated. However, when intermediate phase angles are investigated it becomes clear that environmental factors, particularly oxidation, play a significant role in the TMFCG rates in RR1000. Previous work by Pretty et al [12] showed that the direction of the TMF cycle, **Figure 11,** in stress-temperature space (clockwise (CW), +90°, or anticlockwise (ACW), -90°) affected crack growth rates in FG RR1000, **Figure 12a,** since despite the temperature at peak stress being equivalent in the two tests, changes in failure mode and gradient of the Paris curve were clearly apparent. This was explained through the fact that in the CW cycle the specimen is unloaded at high temperatures, allowing for oxidation of grain boundaries ahead of the crack tip, along which the crack then grows when loaded under tension at low temperatures. In the ACW case

the tensile loading takes place at high temperatures and as such strain rate plays a significant role in the fracture. In a relatively fast cycle (80 seconds) the failure mode is transgranular since dynamic transgranular failure progresses faster under these conditions than the oxidation process. However, if the cycle time is increased to 500 seconds then the oxidation process overtakes the dynamic transgranular failure and the failure mode reverts to intergranular.

In terms of crack growth rates, this effect can be seen in FG RR1000 in **Figure 12a**. The shallower gradient of the CW test is an indicator of the more dominant oxidation process, whereas in the ACW test an increase in stress intensity range, ΔK, leads to a more marked increase in crack growth rate. **Figure 12b** shows that similar trends are seen in CG RR1000, albeit with an increased temperature cycle (400-750°C) when compared to the FG (300-700°C) cycle. Although the peak temperatures differ the trends in the two data sets are broadly comparable due to the increased temperature capability of the CG material.

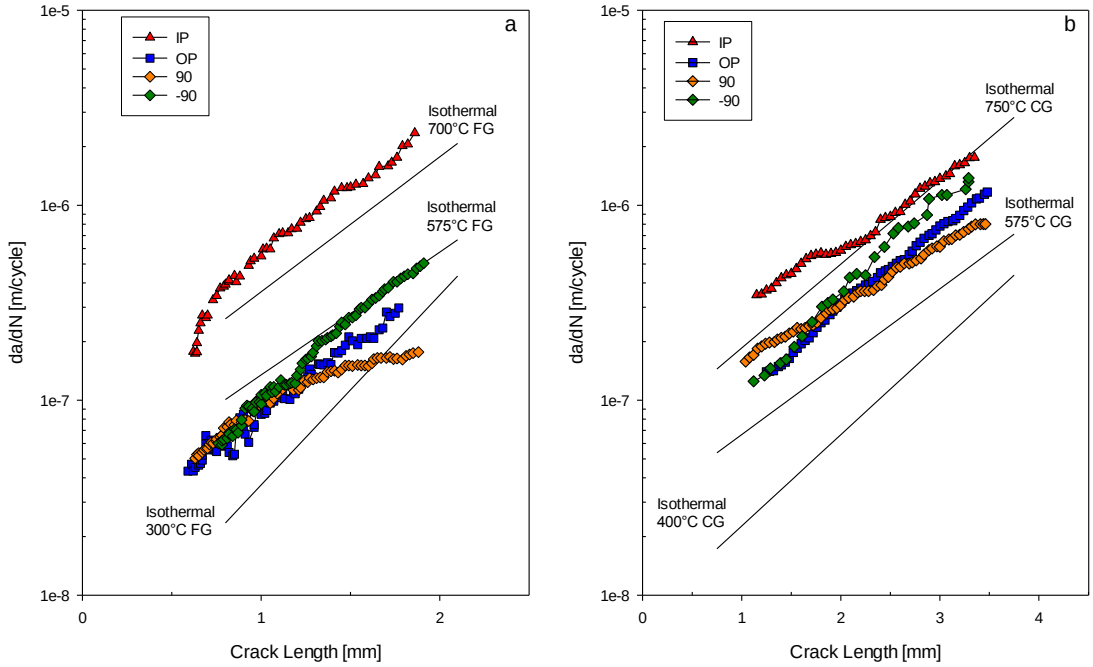

Figure 12: *Effect of phase angle on RR1000 TMFCG rates a) FG variant under 300-700°C temperature range and b) CG variant under 400-750°C. In CW (+90°) cycles, grains ahead of the crack tip oxidise on unloading leading to intergranular failure, whereas in ACW (-90°) cycles, there is a competing process between dynamic fracture and oxidation, which is strain rate dependant.*

Indeed, the improved crack growth resistance of CG RR1000 is evident through its lower growth rates despite the increased peak cycle temperature. It is noticeable however that there is less of a spread in the crack growth data than was seen in the FG material. Presumably this is related to overall greater degrees of interaction between fatigue, creep and environment at this higher temperature, meaning that intermediate phase angle and OP crack growth rates can approach the IP rates. Furthermore, the interaction between fatigue and oxidation is again evident. It is noticeable that at lower ΔK values the CW 90 shows a shallow gradient, indicative of the dominance of oxidation. However, as the crack length (a) (and ΔK) increases, dynamic fracture begins to overtake oxidation, and a steeper gradient in the Paris curve is found. These findings are then supported by **Figure 13**, which shows intergranular fracture in the early stages of crack growth, which then

transitions to transgranular fracture at high ΔK values. Testing at the phase angles of 45° and -135° was shown to be reasonably predictable from both IP and OP data.

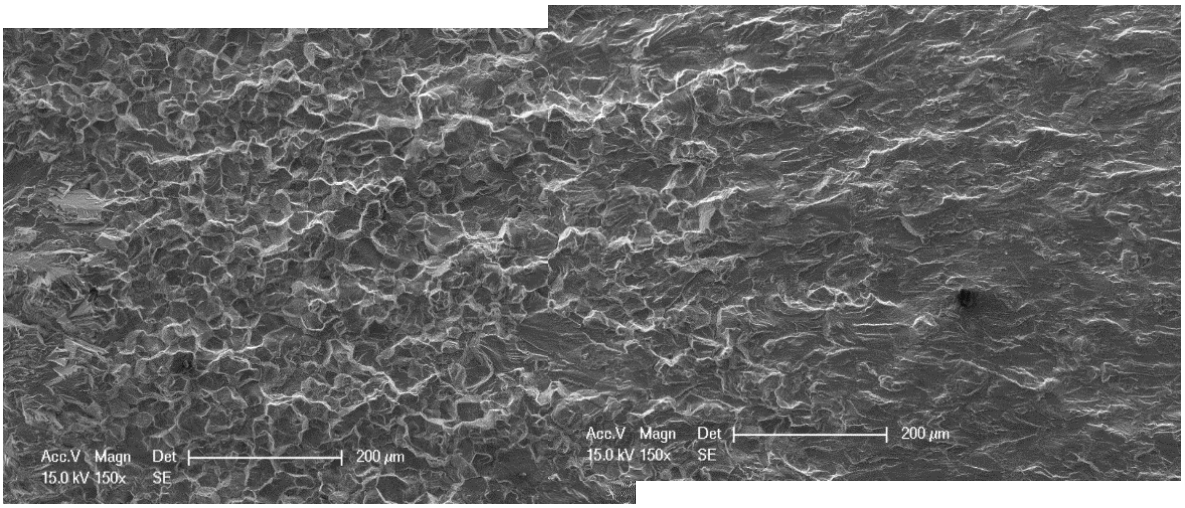

Figure 13: *Fractograph showing the transition from intergranular fracture to transgranular of a CG variant of RR1000 under 400-750°C CW90 cycle.*

Results of crack growth modelling

Initial approaches have been made to attempt to model the TMF crack growth behaviour under IP and OP test conditions. These approaches are based on the crack growth model proposed by Forman [22], Bouvard et al [23] established an extension, which allows the modelling of the crack growth under high temperature and an-isothermal test conditions. This model is based on the assumption of a linear decomposition of total crack growth in fatigue and creep crack growth, where these effects can be calculated independently.

Further details of the methodology are provided in an alternative publication [24]. **Figure 14** shows the prediction of crack growth for a single OP test (left) and IP test (right).

The model is able to predict the total crack growth in good accordance with the experimental data. As shown for the prediction of the OP test in Figure 15 (left), total crack growth rate is mainly driven by fatigue crack propagation, since creep can be neglected at peak load. This fact is supported by the evaluation of the fracture surface which shows a clear transgranular crack propagation as demonstrated in **Figure 10**. As is shown in [24], by evaluation of the numerical results, creep crack growth occurs, but only during short time intervals, where temperature and stress intensity factors support creep propagation. However, this contribution is more than 100 times smaller when compared to the fatigue crack growth, the creep effects in OP testing are negligible.

For IP testing (**Figure 14** (right)), creep crack growth with noticeable magnitude already occurs for normalised stress intensity factors above 1 but the total crack growth is dominated by fatigue crack growth until a normalised stress intensity factor of 2.2 is reached, when creep crack propagation overtakes. This is shown as a crossing of the lines of the separately calculated fatigue and creep crack growth mechanism in **Figure 14** (right). The presence of a creep deformation mechanism is also clearly visible on the distinct intergranular crack propagation shown on the fracture surfaces in **Figure 9** as discussed in the section above. In order to demonstrate the general applicability for crack growth prediction, **Figure 15** shows a summary for all conducted tests with corresponding numerical simulation.

The application of the crack growth model to OP tests show excellent agreement with the experimental data. However, the prediction of IP testing is only practicable for some tests as shown in **Fig 15**. As it is mentioned in **Figure 6** above as well as in the literature [21], crack growth under high temperature is highly influenced by microstructural aspects, i.e. the size distribution of secondary and tertiary γ'.

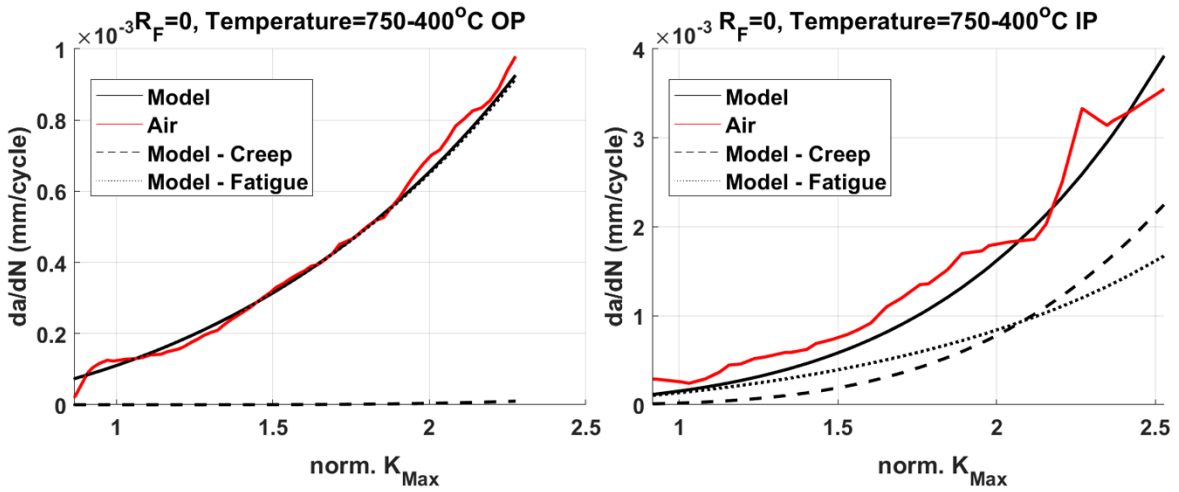

Figure 14: *Crack growth prediction for OP (left) and IP (right) test under thermo-mechanical fatigue loading.*

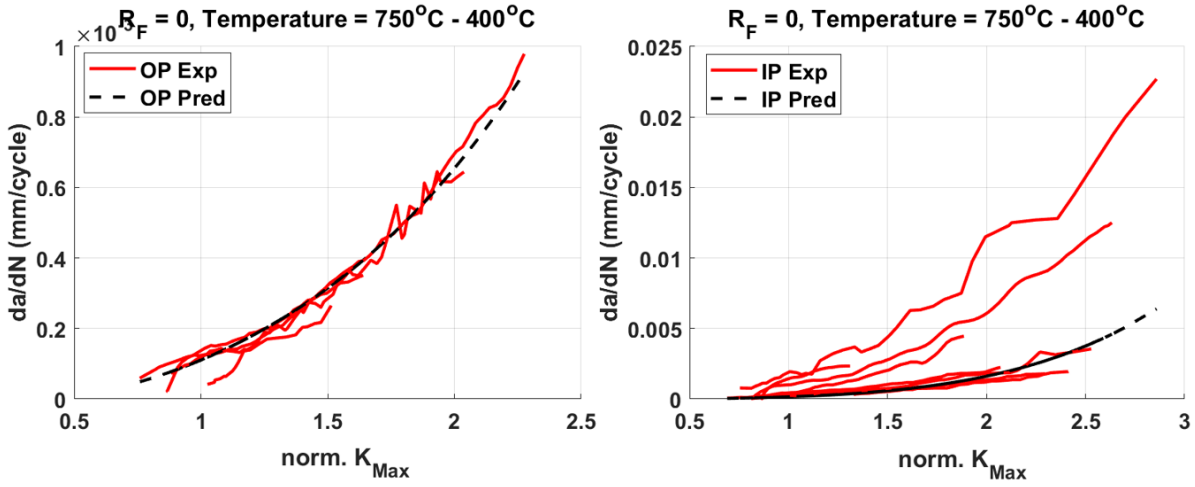

Figure 15. *Summary for numerical crack growth prediction for all conducted OP tests (left) and IP tests (right).*

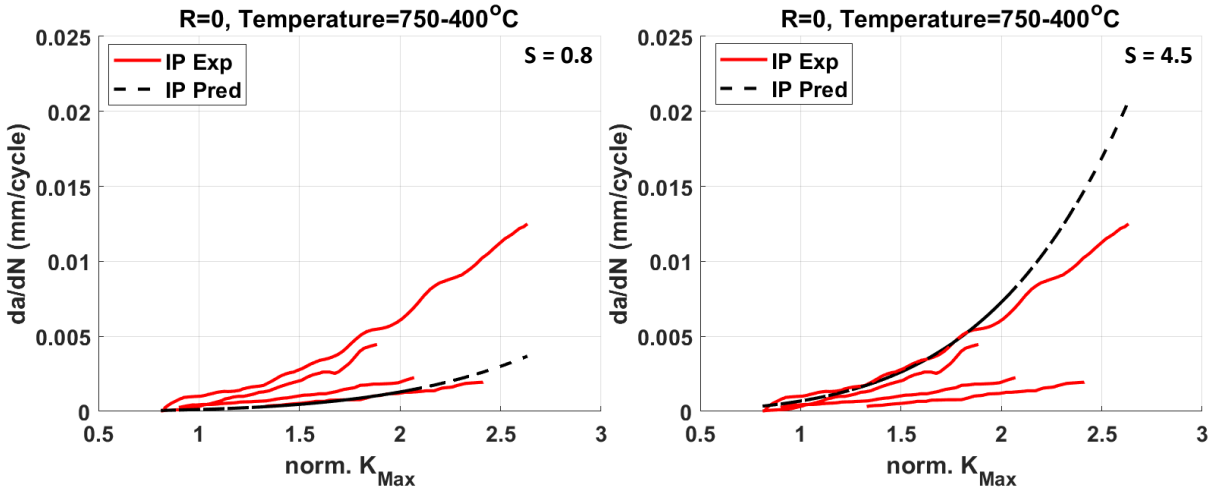

Figure 16: *Prediction of IP TMF crack growth rates as a function of secondary and tertiary γ' sizes.*

In order to model the influence of the γ' size distribution i.e. microstructure on IP tests, a new parameter, S, is introduced. S acts as a multiplier (fitting variable), which influences the crack growth rate during simulation, as a function of secondary and tertiary γ' sizes. Optimisation procedures were carried out to the crack growth tests mentioned in **Figure 6** in order to find corresponding S values, which fit the experimental data in good accordance. Afterwards a power law function was fitted to S and the average secondary and tertiary γ' sizes to establish a mathematical relationship between these parameters. **Figure 16** shows the prediction of the IP tests in dependence of S, for the purpose of considering microstructural effects.

Due to different size distributions of secondary and tertiary γ', local plastic deformation as well as crack growth behaviour changes. Details of the deformation process can be found in [25, 26]. As can be seen in **Figure 16**, an increase in S, which represents in average decrease in the precipitation size, leads to faster crack growth and to good agreements with the experimental data. Furthermore, on the basis of additional optimization processes to determine S from tests without microstructural investigations, prediction about the average sizes of secondary and tertiary γ' can be performed.

Discussion

As would be expected from isothermal crack growth testing, a clear grain size dependency occurs in RR1000 when considering growth rates under TMF loading. FG RR1000 shows poorer resistance to TMFCG with a peak cycle temperature of 750°C whether testing is conducted IP or OP.

IP crack growth rates have been shown to be extremely sensitive to material microstructure, **Figure 6**, with significant variation found in the IP growth rates in CG RR1000, an effect which has been directly correlated to secondary γ' size. It is interesting that in the worst-case scenario seen in the current work, CG RR1000 begins to approach the growth rates seen in FG RR1000 at the same temperature, reaffirming the effect of microstructure. FG RR1000, with a more controllable grain size shows none of this microstructural variability and therefore provides very consistent crack growth rates. IP crack growth rates increase with peak cycle temperature as would be expected, although this effect is not dramatic in either FG or CG RR1000.

Perhaps more interestingly, a difference has been detected between the behaviour of FG and CG RR1000 when conducting OP TMF crack growth tests. In FG RR1000, peak cycle temperature was not shown to have an effect on OP TMF crack growth rates, whereas in CG RR1000 either an increase in T_{Max} or a dwell period at T_{Max} was shown to consistently increase crack growth rates. Since this

temperature is applied when the specimen is fully unloaded, it is proposed that this increase in crack growth rate is due to relaxation of compressive stresses at the crack tip, hence increasing the mean stress and allowing for a larger strain increment on reloading.

TMF cycles often show interactions between high temperature damage mechanisms, and the interaction of fatigue and creep as described previously in OP cycles can be further complicated in situations where the crack is more open and oxidation is able to penetrate to the crack tip and embrittle grain boundaries ahead of this. Clear evidence of this has been found in the differences between CW (+90°) and ACW (-90°) with oxidation now playing a clear role in the crack propagation. Although the contributions of oxidation have manifested themselves slightly differently in the two grain size variants, the differences between the two cycles are summarised in **Figure 17** and **Figure 18**. The diagrams have been constructed to provide a visual representation of the damage mechanisms involved under TMF loading for different phase angles. The transition in colour between blue and red represents the increasing temperature in the cycle, while the interior schematics highlight the crack opening under stress and the impact on fracture mode. For FG material the crack growth is dominated throughout by oxidation, resulting in intergranular failure, whereas in CG material a transition occurs towards higher ΔK values where the mechanism reverts to transgranular failure as dynamic fracture overtakes the oxidation process.

Early approaches to modelling the TMF data have also been encouraging. The current model is able to predict OP TMF crack growth tests with high accordance to the experimental data. This is due to the fact of low level of experimental scatter, which can attribute to less sensitivity to microstructure during crack propagation. However, IP TMF crack growth shows a high dependency on the microstructure. By using the size dependent parameter S, calibrated on microstructural investigations, crack growth tests can be predicted with good accuracy. Furthermore, it is also possible with additional optimisation procedures to predict the size distribution for further tests.

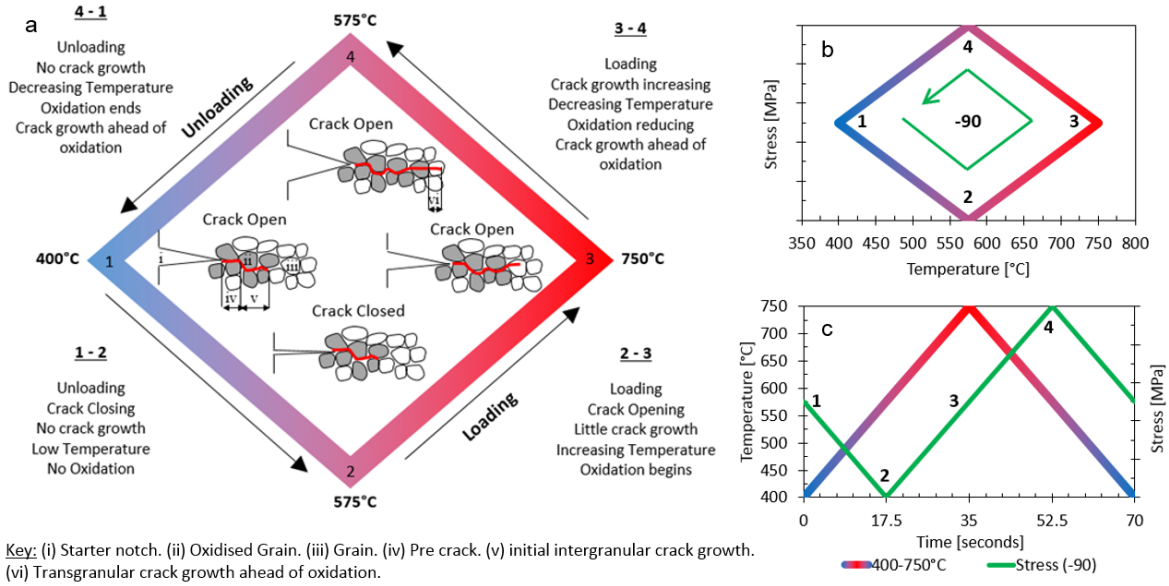

Key: (i) Starter notch. (ii) Oxidised Grain. (iii) Grain. (iv) Pre crack. (v) initial intergranular crack growth. (vi) Transgranular crack growth ahead of oxidation.

Figure 17: *a) Damage mechanisms in ACW (-90°) TMF cycle, 400-750°C, b) Stress-temperature waveform, c) Applied cyclic waveforms, strain-time shown in green, temperature-time shown in red/blue.*

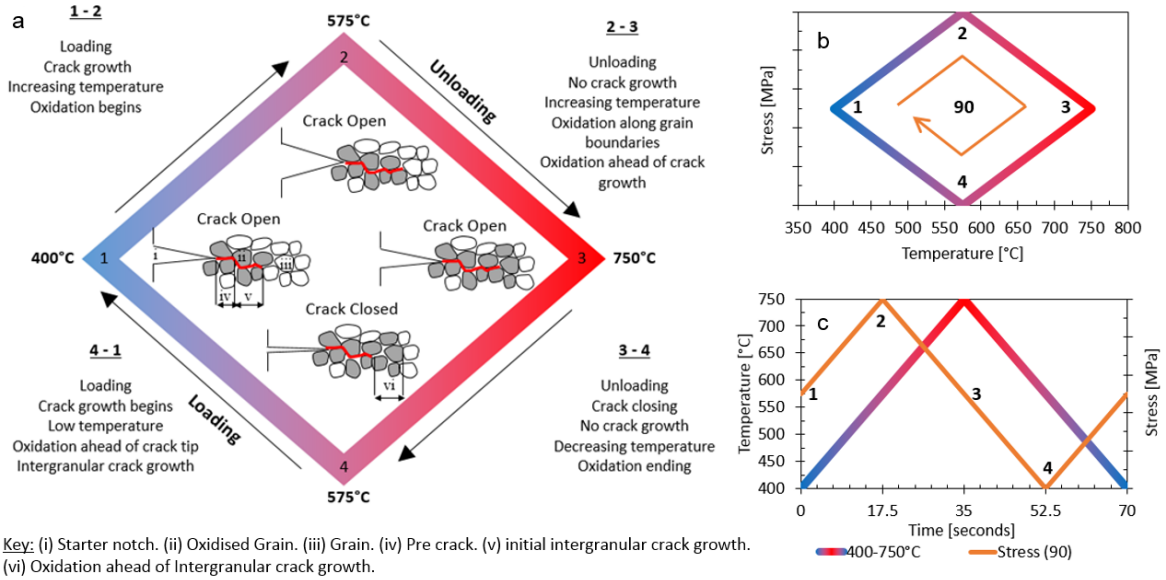

Key: (i) Starter notch. (ii) Oxidised Grain. (iii) Grain. (iv) Pre crack. (v) initial intergranular crack growth. (vi) Oxidation ahead of Intergranular crack growth.

Figure 18: *a) Damage mechanisms in CW (+90°) TMF cycle, 400-750°C, b) Stress-temperature waveform, c) Applied cyclic waveforms, strain-time shown in orange, temperature-time shown in red/blue.*

Conclusions

Extensive thermo-mechanical fatigue crack growth testing has been conducted using recently developed experimental facilities at Swansea University and has allowed for detailed evaluation of the effects of phase angle on two grain size variants of RR1000. The following conclusions have been drawn:-

- Similar to isothermal experiments, the grain size of the material is related to crack growth rates. The smaller the grain size the faster the growth rate over all phase angles, as there is less microstructural resistance to the propagation of the crack. The effect is further accentuated under in-phase loading as creep and environmental damage contribute more strongly to crack growth in the FG material.
- In CG RR1000, the In-Phase TMF crack growth rates are highly sensitive to the material microstructure. A direct correlation between secondary γ' size and crack growth rate has been determined for these tests.
- Over the temperatures used in this research, changes of 50°C to the minimum cycle temperature from 400 to 350°C had no effect on TMF crack growth rates. For IP tests this is because crack growth is dominated only by the deformation mechanisms active at high temperature, whereas in OP tests the crack growth rates associated with isothermal testing at 350°C and 400°C did not differ enough to change the crack growth rates.
- Increasing the peak cycle temperature accelerates IP crack growth rates as would be expected. However, this increase in peak cycle temperature showed an increase in OP crack growth rates, but only in the CG RR1000 material. With no evidence of increased oxidation formation on the fracture surface it is suggested that stress relaxation of high compressive stresses at the crack tip accelerates the crack growth rate when the specimen is reloaded. The effect is not seen in FG RR1000, potentially due to the different strain hardening behaviour of the two grain size variants.
- In diamond cycles, CW and ACW, different crack growth rates can be found despite the same overall cycle in stress-temperature space. A schematic approach has been developed to help

understand the role of oxidation in the process and it's interaction with dynamic fracture. It is found that this relationship is dependent on both strain rate and stress intensity range and has manifested itself differently in each grain size variant.

A TMF crack growth model for RR 1000 was developed, based on the work proposed by Bouvard et al [23] for an-isothermal test condition. Early attempts show promise and are dealt with further in alternative publications. However, good correlation is shown here with the OP test data, and a size dependent parameter has been utilised in order to account for the dependence of the IP crack growth rates on secondary γ' size.

Acknowledgements

This project has received funding from the European Union's Horizon 2020 research and innovation programme and Joint Undertaking Clean Sky 2 under grant agreement No 686600. The authors are also grateful for the supply of material and input from Rolls-Royce plc.

References

[1] R.J. Lancaster, M.T. Whittaker, S.J. Williams, A review of thermo-mechanical fatigue behaviour in polycrystalline nickel superalloys for turbine disc applications, Materials at High Temperatures, 30 (2013) 2-12.

[2] M. Marchionni, H. Klingelhöffer, H.J. Kühn, T. Ranucci, K. Matzak, Thermo-Mechanical Fatigue of the Nickel–Base Superalloy Nimonic 90, Key Engineering Materials 345-346 (2007) 347-350.

[3] P. Hähner, E. Affeldt, T. Beck, H. Klingelhöffer, M. Loveday, C. Rinaldi, Validated Code-of-Practice for Thermo-Mechanical Fatigue Testing, EUR 22281 EN, (2006).

[4] M. Okazaki, T. Koizumi, Crack propagation of steels during low cycle thermal-mechanical and isothermal fatigue at elevated temperatures, Metallurgical Transactions A, 14 (1983) 1641-1648.

[5] N.J. Marchand, R.M. Pelloux, B. Ilschner, A fracture mechanics criterion for thermal-mechanical fatigue crack growth of gas turbine materials, Engineering Fracture Mechanics, 31 (1988) 535-551.

[6] B.L. A. Gemma, G. Leverant, Thermomechanical Fatigue Crack Propagation in a Ansiotropic Nickel-Base Superalloy, ASTM STP 612, (1976) 199-213.

[7] P. Hahner, C. Rinaldi, V. Bicego, E. Affeldt, T. Brendel, H. Andersson, T. Beck, H. Klingelhoffer, H. Kuhn, A. Koster, Research and development into a European code of practice for strain controlled thermo-mechanical fatigue testing, International Journal of Fatigue, 30 (2008) 372-381.

[8] D.G. J. Moverare, Hold-time effect on the thermo-mechanical fatigue crack growth behaviour of Inconel 718, Materials science Engineering A, 528 (2011) 8660-8670.

[9] J.J. Moverare, P. Kontis, S. Johansson, R.C. Reed, Thermomechanical fatigue crack growth in a cast polycrystalline superalloy, MATEC Web of Conferences, 14 (2014) 19004.

[10] J. Palmer, J. Jones, A. Dyer, R. Smith, R. Lancaster, M. Whittaker, Development of test facilities for thermo-mechanical fatigue testing, International Journal of Fatigue, 121 (2019) 208-218.

[11] D. Ewest, P. Almroth, B. Sjödin, K. Simonsson, D. Leidermark, J. Moverare, A modified compliance method for fatigue crack propagation applied on a single edge notch specimen, International Journal of Fatigue, 92 (2016) 61-70.

[12] C. Pretty, M. Whittaker, S. Williams, Thermo-Mechanical Fatigue Crack Growth of RR1000, Materials, 10 (2017) 34.

[13] R.J. Mitchell, J.A. Lemsky, R. Ramanathan, H.Y. Li, K.M. Perkins, L.D. Connor, Process Development & Microstructure & Mechanical Property Evaluation of a Dual Microstructure Heat

Treated Advanced Nickel Disc Alloy, in: Roger Reed, K.A. Green (Eds.) Superalloys 2008, TMS, Pennsylvania, 2008.
[14] N. Jones, K. Christofidou, P. Mignanelli, J. Minshull, M. Hardy, H. Stone, Influence of elevated Co and Ti levels on polycrystalline powder processed Ni-base superalloy, Materials Science and Technology, 30 (2014) 1853-1861.
[15] J. Jones, Enhancing the Accuracy of Advanced High Temperature Mechanical Testing through Thermography, Applied Sciences, 8 (2018) 380.
[16] ASTM, Standard Test Method for Measurement of Fatigue Crack Growth Rates, in: E647 - 15e1.
[17] ASTM, Standard Practice for Strain Controlled Thermomechanical Fatigue Testing, in: E2368-10, 2010.
[18] ISO, Metallic materials, Fatigue testing, Strain-controlled thermomechanical fatigue testing method, in: ISO 2011:12111, 2011, pp. 25.
[19] A.S. S. Brookes, H. Klingelhöffer, M. Whittaker, M. Loveday, A.Scholz, A. Wisby, N. Ryder, R. Lohr, S. Stekovic, J. Moverare, S. Holdsworth, D. Dudzinski., Code of Practice for FORCE-CONTROLLED THERMO-MECHANICAL FATIGUE TESTING, TMF-STANDARD 2 Project, (2015) 32.
[20] J. Jones, M. Whittaker, R. Lancaster, S. Williams, The influence of phase angle, strain range and peak cycle temperature on the TMF crack initiation behaviour and damage mechanisms of the nickel-based superalloy, RR1000, International Journal of Fatigue, 98 (2017) 279-285.
[21] H.Y. Li, J.F. Sun, M.C. Hardy, H.E. Evans, S.J. Williams, T.J.A. Doel, P. Bowen, Effects of microstructure on high temperature dwell fatigue crack growth in a coarse grain PM nickel based superalloy, Acta Materialia, 90 (2015) 355-369.
[22] R.G. Forman, V.E. Kearney, R.M. Engle, Numerical Analysis of Crack Propagation in Cyclic-Loaded Structures, Journal of Basic Engineering, 89 (1967) 459-463.
[23] J.L. Bouvard, F. Gallerneau, P. Paulmier, J.L. Chaboche, A phenomenological model to predict the crack growth in single crystal superalloys at high temperature, International Journal of Fatigue, 38 (2012) 130-143.
[24] B. Engel, The prediction of crack propagation in coarse grain RR1000 using a unified modelling approach, International Journal of Fatigue, Submitted (2019).
[25] B.M.B. Grant, E. Knoche, M. Preuss, J.Q. da Fonseca, M.R. Daymond, The Effect of Lattice Misfit on Deformation Mechanisms at High Temperature, Advanced Materials Research, 278 (2011) 144-149.
[26] E.M. Francis, B.M.B. Grant, J.Q.d. Fonseca, P.J. Phillips, M.J. Mills, M.R. Daymond, M. Preuss, High-temperature deformation mechanisms in a polycrystalline nickel-base superalloy studied by neutron diffraction and electron microscopy, Acta Materialia, 74 (2014) 18-29.